Split northern westerlies during the Little Ice Age

Chuan-Chou Shen (river@ntu.edu.tw)
National Taiwan University
John Chiang
University of California, Berkeley https://orcid.org/0000-0001-7723-9544
Valerie Trouet
Uninversity of Arizona https://orcid.org/0000-0002-2683-8704
Véronique Michel
Université Côte d'Azur, CNRS, CEPAM
Hsien-Chen Tsai
Nationa Taiwan University
Patricia Valensi
UMR7194 CNRS
Christoph Spötl
University of Innsbruck https://orcid.org/0000-0001-7167-4940
Elisabetta Starnini
Università di Torino
Marta Zunino
Grotte di Toirano, Toirano (Savona), Italy
Wei-Yi Chien
Nationa Taiwan University
Wen-Hui Sung
Nationa Taiwan University
Yu-Tang Chien
National Science and Technology Center for Disaster Reduction https://orcid.org/0000-0001-5782-4623
Ping Chang
Texas A&M University https://orcid.org/0000-0002-9085-0759
Robert Korty
Texas A&M University
Hsun-Ming Hu
National Taiwan University

Article

Keywords:

Posted Date: March 18th, 2022

DOI: https://doi.org/10.21203/rs.3.rs-1348259/v1

Version of Record: A version of this preprint was published at Nature Communications on August 20th, 2022. See the published version at https://doi.org/10.1038/s41467-022-32654-w.

Split northern westerlies during the Little Ice Age

Hsun-Ming Hu[1,2], John C. H. Chiang[3], Valerie Trouet[4], Véronique Michel[5,6], Hsien-Chen Tsai[1,2], Patricia Valensi[7], Christoph Spötl[8], Elisabetta Starnini[9], Marta Zunino[10], Wei-Yi Chien[1,2], Wen-Hui Sung[1,2], Yu-Tang Chien[11], Ping Chang[12], Robert Korty[12] and Chuan-Chou Shen[1,2]*

[1]High-Precision Mass Spectrometry and Environment Change Laboratory (HISPEC), Department of Geosciences, National Taiwan University, Taipei 10617, Taiwan, ROC

[2]Research Center for Future Earth, National Taiwan University, Taipei 10617, Taiwan, ROC

[3]Department of Geography, University of California, Berkeley, CA, USA

[4]Laboratory of Tree-Ring Research, University of Arizona, AZ, 85721, USA

[5]Université Côte d'Azur, CNRS, CEPAM, 06300 Nice, France

[6]Université Côte d'Azur, CNRS, OCA, IRD, Géoazur, 06560, Valbonne, France

[7]HNHP, UMR 7194, Sorbonne Universités, MNHN, CNRS, UPMC, UPVD, Paris, France; Musée de Préhistoire, 06690 Tourrette-Levens, France

[8]Institute of Geology, University of Innsbruck, Innrain 52, 6020 Innsbruck, Austria

[9]Department of Civilizations and Forms of Knowledge, University of Pisa, Via dei Mille 19, 56126 Pisa, Italy & Archaeological Superintendency of Liguria, Via Balbi 10, 16126 Genova, Italy

[10]Toirano Cave, Piazzale D. Maineri 1, 17055, Toirano (SV), Italy

[11]National Science and Technology Center for Disaster Reduction, New Taipei City 23143, Taiwan.

[12]Texas A&M University, College Station, Texas

* Correspondence and requests for materials should be addressed to: Chuan-Chou Shen (river@ntu.edu.tw).

Abstract: The Little Ice Age (LIA) was the coldest period of the past millennium, characterized by high-density volcanism, low solar activity, and increased Northern Hemisphere sea-ice cover. Past studies of LIA circulation changes over the North Atlantic sector have typically referenced the North Atlantic Oscillation (NAO), though recent studies have noted that LIA climate patterns appear to be possess complexity not captured by an NAO analog. Here, we present a new precipitation-sensitive stalagmite record from northern Italy that covers the past 800 years at high resolution. Combined with terrestrial and marine records in the North Atlantic realm, we show that in the early LIA (1470-1610 C.E.), a multi-decadal scale atmospheric blocking over northern Europe split the westerlies away from central and northern Europe, and towards the Arctic and the Mediterranean. This enhanced blocking results in a cold and dry climate over central and northern Europe, and wetter conditions over the Mediterranean. The LIA atmospheric blocking could be caused by the concurrent sea-ice reduction in the Arctic and the Spörer solar minimum. With ongoing ice melting in the northern high latitudes and decreasing solar irradiance in the coming years, the early LIA may potentially serve as an analog for European hydroclimatic conditions in the coming decades.

Main Text:

In the North Atlantic sector, the westerlies, as part of this large-scale air current, transport moisture to Europe, primarily during the winter half year (October-March). The path and strength of the westerlies can be controlled by the relative strength between the Icelandic Low and the Azores High, known as the North Atlantic Oscillation (NAO; 1). The frequency of atmospheric blockings, i.e., persistent and stationary high-pressure systems that block the westerlies for several days to weeks (2), can also prevent the transport of warm and moist air masses to Europe in winter, leading to cold spells in Europe, such as the winter of 2010 C.E. (3,4). Scandinavia blocking (5-7) in particular plays an important role in extreme weather (4) through modulating the trajectory of the westerlies (6). To better understand the variability in the westerlies and the complexity of the atmospheric blockings at different timescales, natural archives that extend back beyond the instrumental era are needed.

Several proxy records have recorded variability in the westerlies over the past millennia (e.g., 8,9). The Little Ice Age (LIA; ca. 1450-1850 C.E.; 10) was the coldest episode of the past millennium and featured low solar irradiance, high variability in sea ice extent, and frequent volcanic eruptions (11,12). It was further characterized by enhanced atmospheric blocking over Greenland, which indicates a negative phase of the North Atlantic Oscillation (NAO) (e.g., 8,13). However, model simulations do not always support these proxy-based results (14,15). The discrepancy between model results and paleoclimate reconstructions can be attributed to the non-stationarity of the NAO, i.e., spatial and intensity changes of the NAO dipole between the Icelandic Low and the Azores High (9,15). The non-stationarity of the NAO can be caused by blockings over the North Atlantic realm, which change the route of the westerlies and result in complex precipitation patterns over mainland Europe (16-18). However, so far, there are few climate records directly documenting the westerly routes that hampers our understanding of the Atlantic climate evolution in the LIA. Here, we present a new autumn-winter precipitation-sensitive stalagmite-based record from northern Italy that spans the past 800 years at high resolution. Combined with previously published climate proxies from Europe and northern Africa, our results document split westerlies caused by a persistent atmospheric blocking event over northern Europe during a neutral to positive NAO phase at the beginning of the LIA. This climate pattern has an analog in the modern-day wintertime circulation, the Scandinavian pattern.

Material and Methods. Bàsura cave (44.13 ˚N, 8.2 ˚E), featuring a Mediterranean climate with dry summers and humid winters, is located in Toirano, northern Italy (Fig. S1). Over 70% of the annual precipitation, 1269 (±331) mm (1σ, 1950-2008 C.E.; Genoa meteorological station; 44.41 ˚N, 8.93 ˚E, 55 m above sea level [a.s.l.], 70 km northeast of Toirano), falls during the rainy season from September to February (Sep-Feb). The interior of the 1 km-long cave experiences 97-100% relative humidity and a stable annual temperature of 15.6 ˚C. Stalagmite BA18-4 (Fig. S2) was collected in a narrow chamber 350 m from the main entrance in 2018 C.E. X-ray diffraction analysis shows that this stalagmite is composed of calcite. Its chronology was established using StalAge (19) based on 15 U-Th dates (20), measured on a Thermo-Finnigan Neptune multi-collector inductively coupled plasma mass spectrometer (21). A total of 214 subsamples were drilled for Mg, Sr and Ba and analyzed using external matrix-matched standards for every 4-5 samples on an inductively coupled plasma sector-field mass spectrometer (ICP-SF-MS, Finnigan Element II, 22) (Data S1), with a two-sigma reproducibility of ±0.5%.

Bàsura records. Over the past 750 years, Bàsura Mg/Ca, Sr/Ca and Ba/Ca vary between 20-30 mmol/mol, 0.35-0.55 mmol/mol, and 4.0-8.0 μmol/mol, respectively (Fig. S3). The trace element/calcium (Me/Ca) ratio in stalagmites is a proxy of hydroclimate above the cave modulated by prior calcite precipitation (PCP)(23-25). PCP, i.e. precipitation of calcite in the karst aquifer before the drip water reaches the stalagmite, is enhanced during dry climate conditions due to reduced recharge, long residence time, and low CO_2 concentration in the cave air. Covariation of Me/Ca ratios (Mg/Ca, Sr/Ca and Ba/Ca) in the stalagmite and in drip water suggests a strong PCP effect when the partition coefficients ($D_{Me} = (Me/Ca)_{calcite}/(Me/Ca)_{drip\ water}$) of these elements are less than one (26). In the Bàsura stalagmite, Ba/Ca and Sr/Ca ratios are strongly positively correlated ($R^2 = 0.90$, Fig. S4A), indicating a strong PCP effect. A lower correlation coefficient ($R^2 = 0.59$) for Mg/Ca versus Sr/Ca (Fig. S4B) suggests additional controls on Mg/Ca.

The inconsistency between Mg/Ca and Sr/Ca can be potentially attributed to a temperature effect (23-26). For example, both Northern Hemisphere temperature records (Fig. S3A; 27) and Bàsura Mg/Ca (Fig. S3B) show a clear decreasing multidecadal trend from 1500 to 1600 C.E. and an increasing trend from 1850 C.E. onwards, suggest a temperature effect on stalagmite Mg/Ca. Stalagmite Mg/Ca variations were also proposed to be affected by the source effect in the Mediterranean region (30). Strong westerly winds could lead to the deposition of Mg-enriched particles (derived from dolomite-dominated coastal regions) in the catchment of the cave and a resulting high Mg/Ca ratio in the speleothem. Compared to Mg/Ca, Sr/Ca and Ba/Ca are less influenced by temperature (23-26) and thus are more suitable for reconstructing paleohydrology. Bàsura Sr/Ca is indeed significantly negatively correlated with instrumental precipitation records from the weather stations of Genoa (44.41 ˚N, 8.93 ˚E, 55 m above sea level, a.s.l.), Milan (45.47 ˚N, 9.19 ˚E, 150 m a.s.l.), and Nice (G/M/N) (43.65 ˚N, 7.21 ˚E, 2 m a.s.l.) from September to February (autumn-winter) for 1855-1965 C.E. within dating uncertainties (Fig. S5). The Sr/Ca and Ba/Ca records are strongly positively correlated (Figs. S3C and D, S4A) and both indicate the extent of the PCP effect and we therefore use Bàsura stalagmite Sr/Ca record to represent Toirano precipitation history to simplify our discussion.

Southern European precipitation pattern. Toirano autumn-winter precipitation is strongly related to variability in autumn-winter North Atlantic sea-level pressure (20). Instrumental autumn-winter precipitation data averaged for the G/M/N stations (1950-2008 CE) show a strong positive correlation with sea-level pressure (SLP) anomalies with a ridge over Scandinavia and a trough over the western Europe (Fig. 1A, shades). The correlation pattern closely resembles the SLP response to the Scandinavian teleconnection index (SCAND, by the

Climate Prediction Center; Fig. 1A, contours; 7). Indeed, G/M/N precipitation is strongly positively correlated with the SCAND index ($r=0.63$, $p < 0.05$, 1950-2020 CE; $n = 70$), suggesting that the SCAND exerts a stronger control on winter precipitation in Toirano. Positive SCAND phases are associated in winter with synoptic high-pressure anomalies over the eastern Scandinavian Peninsula and low pressure anomalies over western Europe. The wind filed analysis (Fig. 1B; vectors) shows that the positive SCAND can lead to a split configuration of the westerlies, with the northern branch tilting towards the Arctic Sea and the southern branch flowing into the Mediterranean. These winds carrying moisture affect the climate in the Greenland and the Mediterranean region (Fig. 1B, shades), with increasing (decreasing) precipitation in northern Mediterranean/SE Greenland (northern Europe).

Beyond daily to seasonal timescales, the frequency of the occurrences of atmosphere blocking patterns, though only existing for a few days to 1-2 weeks at a time, significantly affects the climate (31, 32). On decadal-to-centennial timescales, the frequency of blocking events can even change the position of the NAO SLP dipole and the route of the westerlies (31, 32). For example, frequent occurrences of blockings over Greenland can result in an equatorial migration of the westerlies (33). Similarly, the frequent occurrence of blockings over Scandinavia that characterize positive SCAND phases can lead to a split in the westerlies, with its southern branch penetrating into southern Europe (Fig. 1B) (6) and bringing high precipitation to Toirano and Bàsura cave. Thus, the precipitation histories documented in Bàsura stalagmites reflect the variability of atmospheric pressure systems over the North Atlantic and particularly of the SCAND teleconnection.

Little Ice Age. During the LIA (ca. 1450-1850 C.E.), the climate in the North Atlantic/European realm was mostly cold and dry (10,13,15), but proxy records show considerable variability on multi-decadal to centennial time scales within this period. The potassium ion record in a Greenland ice core (34; Fig. 2A) suggests that the westerlies over the North Atlantic were strong from 1470 until 1610 C.E., concurrent with a neutral-positive NAO mode as indicated by a composite NAO reconstruction (Fig. 2A; 9). However, the stalagmite-based winter precipitation record of Roaring cave (35)(Fig. 2C, green) and the aeolian sediment Bromine record from Scotland (28)(Fig. 2C; mustard) suggest that the British Islands experienced a relatively dry and less windy climate during this interval. Dry and cold conditions are also inferred for western Germany, based on stalagmite $\delta^{18}O$ data from Bunker cave (Fig.

2D; 36,37) and for high-latitude Norway, based on stalagmite $\delta^{18}O$ data (38; S5A) and lacustrine records (39). The precipitation and wind minima in these regions do not corroborate a neutral-positive NAO mode (35). On the other hand, warm and humid conditions during this 140-yr interval in central Europe are documented by a stalagmite $\delta^{18}O$ record from Spannagel cave, Austria (Fig. 2E; 40) and by our stalagmite Sr/Ca record from Bàsura cave (Fig. 2F). Similar warm and wet conditions are further registered by stalagmite records from Portugal (29; Fig. S6B), Spain (41; Fig. S6C), and Turkey (42; S6D; Fig. 3G), while stalagmite records from Morocco record a dry interval (Figs. 2G and S6F; 43,44).

Pressure anomaly during 1470-1610 C.E. The dry/cold climate in northern Europe during 1470-1610 C.E. can be reconciled with a neutral-positive NAO phase (Fig. 2B; 9) by Scandinavian blockings. Our Bàsura record suggests that during this early LIA period (1470-1610 C.E.), the westerlies were blocked over northern Europe by a positive pressure anomaly, whereas the windy/warm/humid climate over southeastern Greenland, as well as over southern Europe suggests that the split westerlies were diverted in these directions (Fig. 2H). Such climate setting is similar to the anomalously wet conditions in southeastern Greenland and the northwestern Mediterranean during positive SCAND phases (Fig. 1B). This mechanism can explain the simultaneous drying over northern Europe and wettening over Greenland and southern Europe (Fig. 2H; 6,45). The positive SCAND phase does not explain the drying over North Africa, but given that the NAO phase was neutral-positive (Fig. 2B; 9) during 1470-1610 C.E., the dry climate in northern Africa could be attributed to an enhanced Azores High that prevented the moisture tracking into Morocco.

Co-incidence with reduced sea ice and solar forcing. Ice-rafted debris (IRD) records from the Fram Strait (Fig. 3B; 46), foraminiferal-inferred sea-ice records on the North Greenland shelf (Fig. 3B; 47), and diatom-based sea-ice reconstructions from the west Greenland shelf (Fig. 3C; 48) all show a large sea-ice cover in North Atlantic preceding the LIA during the middle to late 1300s, presumably induced by intense volcanism (Fig. 3A; 49) and low solar irradiance (Fig. 3G; 50)(e.g., 11,51). Extensive sea ice in the North Atlantic triggered a cooling in Europe starting around 1400 C.E. by changing ocean circulation (12,52). Sea ice extent then significantly decreased in the 1400s C.E (Fig. 3B-C) due to an intrusion of warm Atlantic Water into the North Atlantic (53), reflected by a positive phase of the Atlantic Multidecadal Variability (Fig. 3G; 54). Indeed, the Scandinavian blocking we infer during 1470-1610 C.E.

matches, within dating uncertainties, the previously identified North Atlantic “decreased sea ice extent” event between 1470-1610 C.E. (Fig. 3D, red bar; 55). Simulated results also indicate a reduction of North Atlantic sea ice during the early part of this period (1470-1520 C.E.), especially in the Barent-Kara sea (56). The loss in sea ice in the Barent-Kara sea can trigger a positive pressure anomaly over Scandinavia (57,58). Reduced sea ice results in a heat flux anomaly in the low-level atmosphere that excites the stationary Rossby wave propagating towards the southeast, i.e., increasing the blocking frequency in northern Europe (59-61). The Scandinavian blocking during 1470-1610 C.E. suggested by our results (Fig. 2G) could be triggered by the reduced sea-ice extent through this ocean-atmosphere feedback.

The atmospheric blocking in the early LIA could have been further exacerbated by low solar irradiation (Fig. 3G). Model simulations (62,63) and proxy records (64) suggest that solar irradiation changes can have a significant effect on ozone chemistry in the stratosphere that disturbs the polar vortex and thus influences the tropospheric jet stream and atmospheric circulation (e.g., 62-66). Our Bàsura stalagmite Sr/Ca data, decreasing from 0.055 mmol/mol at 1460 C.E. to 0.035 mmol/mol at 1550 C.E., suggests that Scandinavian blocking progressively strengthened during this interval (Fig. 3E). This 90-yr interval broadly matches the Spörer Minimum (1460-1550 C.E., Fig. 3G; 67), supporting this linkage between atmospheric changes and solar variability.

The decreased sea ice extent from 1450-1620 C.E. is more pronounced than that during the Medieval Climate Anomaly (ca. 800-1300 C.E.), and has possibly the longest duration over the past 1400 years (55). Our results present proxy-based evidence of enhanced atmospheric blocking over northern Europe during this interval, potentially in response to the sea ice reduction and also enhanced by solar minimum during the LIA, that persisted for at least several decades. Our results thus potentially provide an insight for the coming decades, when solar variability could result in a “Grand Minimum” (68) and the Arctic is projected to be ice free by 2030 C.E. (69).

References and Notes:

1. J. W. Hurrell. Decadal trends in the North Atlantic Oscillation: regional temperatures and precipitation. *Science* **269**, 676–679 (1995).
2. T. Woollings, D. Barriopedro, J. Methven, S. W. Son, O. Martius, B. Harvey, J. Sillmann, A. R. Lupo, S. Seneviratne, Blocking and its Response to Climate Change. *Curr. Clim. Chang. Reports*. **4**, 287–300 (2018).
3. J. Cattiaux, R. Vautard, C. Cassou, P. Yiou, V. Masson-Delmotte, F. Codron, Winter 2010 in Europe: A cold extreme in a warming climate. *Geophys. Res. Lett.* **37**, 1–6 (2010).
4. L. Brunner, G. C. Hegerl, A. K. Steiner, Connecting atmospheric blocking to European temperature extremes in spring. *J. Clim.* **30**, 585–594 (2017).
5. C. M. Grams, R. Beerli, S. Pfenninger, I. Staffell, H. Wernli, Balancing Europe's wind-power output through spatial deployment informed by weather regimes. *Nat. Clim. Chang.* **7**, 557–562 (2017).
6. E. Madonna, C. Li, C. M. Grams, T. Woollings, The link between eddy-driven jet variability and weather regimes in the North Atlantic-European sector. *Q. J. R. Meteorol. Soc.* **143**, 2960–2972 (2017).
7. A. G. Barnston, R. E. Livezey, Classification, Seasonality and Persistence of Low-Frequency Atmospheric Circulation Patterns. *Mon. Weather Rev.* **115**, 1083–1126 (1987).
8. V. Trouet, J. Esper, N. E. Graham, A. Baker, J. D. Scourse, D. C. Frank, Persistent Positive North Atlantic Oscillation Mode Dominated the Medieval Climate Anomaly. *Science* **324**, 78–80 (2009).
9. P. Ortega, F. Lehner, D. Swingedouw, V. Masson-Delmotte, C. C. Raible, M. Casado, P. Yiou, A model-tested North Atlantic Oscillation reconstruction for the past millennium. *Nature*. **523**, 71–74 (2015).
10. P. Moffa-Sánchez, E. Moreno-Chamarro, D. J. Reynolds, P. Ortega, L. Cunningham, D. Swingedouw, D. E. Amrhein, J. Halfar, L. Jonkers, J. H. Jungclaus, K. Perner, A. Wanamaker, S. Yeager, Variability in the Northern North Atlantic and Arctic Oceans Across the Last Two Millennia: A Review. *Paleoceanogr. Paleoclimatology*. **34**, 1399–1436 (2019).
11. M. W. Miles, C. S. Andresen, C. V. Dylmer, Evidence for extreme export of Arctic sea ice leading the abrupt onset of the Little Ice Age. *Sci. Adv.* **6** (2020),
12. F. Lapointe, R. S. Bradley, Little Ice Age abruptly triggered by intrusion of Atlantic waters into the Nordic Seas. *Sci. Adv.* **7** (2021).

13. V. Trouet, J. D. Scourse, C. C. Raible, North Atlantic storminess and Atlantic Meridional Overturning Circulation during the last Millennium: Reconciling contradictory proxy records of NAO variability. *Glob. Planet. Change*. **84–85**, 48–55 (2012).
14. J. G. Pinto, C. C. Raible, Past and recent changes in the North Atlantic oscillation. *Wiley Interdiscip. Rev. Clim. Chang.* **3**, 79–90 (2012).
15. F. Lehner, C. C. Raible, T. F. Stocker, Testing the robustness of a precipitation proxy-based North Atlantic Oscillation reconstruction. *Quat. Sci. Rev.* **45**, 85–94 (2012).
16. Y.-H. Wang, G. Magnusdottir, H. Stern, X. Tian, Y. Yu, Decadal variability of the NAO: Introducing an augmented NAO index. *Geophys. Res. Lett.* **39** (2012)
17. Y. H. Wang, G. Magnusdottir, The shift of the northern node of the NAO and cyclonic rossby wave breaking. *J. Clim.* **25**, 7973–7982 (2012).
18. G. W. K. Moore, I. A. Renfrew, R. S. Pickart, Multidecadal Mobility of the North Atlantic Oscillation. *J. Clim.* **26**, 2453–2466 (2013).
19. D. Scholz, D. L. Hoffmann, StalAge – An algorithm designed for construction of speleothem age models. *Quat. Geochronol.* **6**, 369–382 (2011).
20. Hu, H.-M. *et al.* The westerly drift over Europe since the middle Holocene. *Nat. Geosci.* In review.
21. C.-C. Shen, C.-C. Wu, H. Cheng, R. Lawrence Edwards, Y.-T. Hsieh, S. Gallet, C.-C. Chang, T.-Y. Li, D. D. Lam, A. Kano, M. Hori, C. Spötl, High-precision and high-resolution carbonate 230Th dating by MC-ICP-MS with SEM protocols. *Geochim. Cosmochim. Acta*. **99**, 71–86 (2012).
22. L. Lo, C. C. Shen, C. J. Lu, Y. C. Chen, C. C. Chang, K. Y. Wei, D. Qu, M. K. Gagan, Determination of element/Ca ratios in foraminifera and corals using cold- and hot-plasma techniques in inductively coupled plasma sector field mass spectrometry. *J. Asian Earth Sci.* **81**, 115–122 (2014).
23. I. J. Fairchild, A. Borsato, A. F. Tooth, S. Frisia, C. J. Hawkesworth, Y. Huang, F. McDermott, B. Spiro, Controls on trace element (Sr-Mg) compositions of carbonate cave waters: Implications for speleothem climatic records. *Chem. Geol.* **166**, 255–269 (2000).
24. I. J. Fairchild, C. L. Smith, A. Baker, L. Fuller, C. Spötl, D. Mattey, F. McDermott, Modification and preservation of environmental signals in speleothems. *Earth-Science Rev.* **75**, 105–153 (2006).

25. J. A. Wassenburg, S. Riechelmann, A. Schröder-Ritzrau, D. F. C. Riechelmann, D. K. Richter, A. Immenhauser, M. Terente, S. Constantin, A. Hachenberg, M. Hansen, D. Scholz, Calcite Mg and Sr partition coefficients in cave environments: Implications for interpreting prior calcite precipitation in speleothems. *Geochim. Cosmochim. Acta*. **269**, 581–596 (2020).
26. I. J. Fairchild, P. C. Treble, Trace elements in speleothems as recorders of environmental change. *Quat. Sci. Rev.* **28**, 449–468 (2009).
27. A. Moberg, D. M. Sonechkin, K. Holmgren, N. M. Datsenko, W. Karlén, S.-E. Lauritzen, Highly variable Northern Hemisphere temperatures reconstructed from low- and high-resolution proxy data. *Nature*. **433**, 613–7 (2005).
28. L. C. Orme, L. Reinhardt, R. T. Jones, D. J. Charman, A. Barkwith, M. A. Ellis, Aeolian sediment reconstructions from the Scottish Outer Hebrides: Late Holocene storminess and the role of the North Atlantic Oscillation. *Quat. Sci. Rev.* **132**, 15–25 (2016).
29. D. L. Thatcher, A. D. Wanamaker, R. F. Denniston, Y. Asmerom, V. J. Polyak, D. Fullick, C. C. Ummenhofer, D. P. Gillikin, J. A. Haws, Hydroclimate variability from western Iberia (Portugal) during the Holocene: Insights from a composite stalagmite isotope record. *The Holocene*. **30**, 966–981 (2020).
30. S. A. Carolin, R. T. Walker, C. C. Day, V. Ersek, R. A. Sloan, M. W. Dee, M. Talebian, G. M. Henderson, Precise timing of abrupt increase in dust activity in the Middle East coincident with 4.2 ka social change. **116** (2019).
31. G. W. K. Moore, I. A. Renfrew, R. S. Pickart, Multidecadal Mobility of the North Atlantic Oscillation. *J. Clim.* **26**, 2453–2466 (2013).
32. L. Comas-Bru, F. Mcdermott, Impacts of the EA and SCA patterns on the European twentieth century NAO-winter climate relationship. *Q. J. R. Meteorol. Soc.* **140**, 354–363 (2014).
33. T. J. Woollings, B. Hoskins, M. Blackburn, P. Berrisford, A new Rossby wave-breaking interpretation of the North Atlantic Oscillation. *J. Atmos. Sci.* **65**, 609–626 (2008).
34. P. A. Mayewski, L. D. Meeker, M. S. Twickler, S. Whitlow, Q. Yang, W. B. Lyons, M. Prentice, Major features and forcing of high-latitude northern hemisphere atmospheric circulation using a 110,000-year-long glaciochemical series. *J. Geophys. Res. Ocean.* **102**, 26345–26366 (1997).

35. A. Baker, J. C. Hellstrom, B. F. J. Kelly, G. Mariethoz, V. Trouet, A composite annual-resolution stalagmite record of North Atlantic climate over the last three millennia. *Sci. Rep.* **5**, 10307 (2015).

36. J. Fohlmeister, A. Schröder-Ritzrau, D. Scholz, C. Spötl, D. F. C. Riechelmann, M. Mudelsee, A. Wackerbarth, A. Gerdes, S. Riechelmann, A. Immenhauser, D. K. Richter, A. Mangini, Bunker Cave stalagmites: An archive for central European Holocene climate variability. *Clim. Past*. **8**, 1751–1764 (2012).

37. S. Waltgenbach, D. F. C. Riechelmann, C. Spötl, K. P. Jochum, J. Fohlmeister, A. Schröder-Ritzrau, D. Scholz, Climate variability in central Europe during the last 2500 years reconstructed from four high-resolution multi-proxy speleothem records. *Geosci.* **11** (2021).

38. H. S. Sundqvist, K. Holmgren, A. Moberg, C. Spötl, A. Mangini, Stable isotopes in a stalagmite from NW Sweden document environmental changes over the past 4000 years. *Boreas*. **39**, 77–86 (2010).

39. K. Vasskog, Ø. Paasche, A. Nesje, J. F. Boyle, H. J. B. Birks, A new approach for reconstructing glacier variability based on lake sediments recording input from more than one glacier. *Quat. Res.* **77**, 192–204 (2012).

40. J. Fohlmeister, N. Vollweiler, C. Spötl, A. Mangini, COMNISPA II: Update of a mid-European isotope climate record, 11 ka to present. *Holocene*. **23**, 749–754 (2013).

41. J. Martín-Chivelet, M. B. Muñoz-García, R. L. Edwards, M. J. Turrero, A. I. Ortega, Land surface temperature changes in Northern Iberia since 4000yrBP, based on $\delta^{13}C$ of speleothems. *Glob. Planet. Change*. **77**, 1–12 (2011).

42. D. Fleitmann, H. Cheng, S. Badertscher, R. L. Edwards, M. Mudelsee, O. M. Göktürk, a. Fankhauser, R. Pickering, C. C. Raible, a. Matter, J. Kramers, O. Tüysüz, Timing and climatic impact of Greenland interstadials recorded in stalagmites from northern Turkey. *Geophys. Res. Lett.* **36**, L19707 (2009).

43. Y. Ait Brahim, H. Cheng, A. Sifeddine, J. A. Wassenburg, F. W. Cruz, M. Khodri, L. Sha, N. Pérez-Zanón, E. H. Beraaouz, J. Apaéstegui, J.-L. Guyot, K. P. Jochum, L. Bouchaou, Speleothem records decadal to multidecadal hydroclimate variations in southwestern Morocco during the last millennium. *Earth Planet. Sci. Lett.* **476**, 1–10 (2017).

44. Y. Ait Brahim, J. A. Wassenburg, L. Sha, F. W. Cruz, M. Deininger, A. Sifeddine, L. Bouchaou, C. Spötl, R. L. Edwards, H. Cheng, North Atlantic Ice-Rafting, Ocean and

Atmospheric Circulation During the Holocene: Insights From Western Mediterranean Speleothems. *Geophys. Res. Lett.* **46**, 7614–7623 (2019).

45. F. Fabiano, H. M. Christensen, K. Strommen, P. Athanasiadis, A. Baker, R. Schiemann, S. Corti, Euro-Atlantic weather Regimes in the PRIMAVERA coupled climate simulations: impact of resolution and mean state biases on model performance. *Clim. Dyn.* **54**, 5031–5048 (2020).
46. J. Müller, K. Werner, R. Stein, K. Fahl, M. Moros, E. Jansen, Holocene cooling culminates in sea ice oscillations in Fram Strait. *Quat. Sci. Rev.* **47**, 1–14 (2012).
47. K. Perner, M. Moros, J. M. Lloyd, E. Jansen, R. Stein, Mid to late Holocene strengthening of the East Greenland Current linked to warm subsurface Atlantic water. *Quat. Sci. Rev.* **129**, 296–307 (2015).
48. L. Sha, H. Jiang, K. L. Knudsen, Diatom evidence of climatic change in Holsteinsborg Dyb, west of Greenland, during the last 1200 years. *Holocene*. **22**, 347–358 (2012).
49. T. J. Crowley, M. B. Unterman, Technical details concerning development of a 1200 yr proxy index for global volcanism. *Earth Syst. Sci. Data*. **5**, 187–197 (2013).
50. E. Bard, G. Raisbeck, F. Yiou, J. Jouzel, Solar irradiance during the last 1200 years based on cosmogenic nuclides. *Tellus B Chem. Phys. Meteorol.* **52**, 985–992 (2000).
51. G. H. Miller, Á. Geirsdóttir, Y. Zhong, D. J. Larsen, B. L. Otto-Bliesner, M. M. Holland, D. A. Bailey, K. A. Refsnider, S. J. Lehman, J. R. Southon, C. Anderson, H. Björnsson, T. Thordarson, Abrupt onset of the Little Ice Age triggered by volcanism and sustained by sea-ice/ocean feedbacks. *Geophys. Res. Lett.* **39**, 1–5 (2012).
52. F. Lehner, A. Born, C. C. Raible, T. F. Stocker, Amplified inception of European little Ice Age by sea ice-ocean-atmosphere feedbacks. *J. Clim.* **26**, 7586–7602 (2013).
53. R. F. Spielhagen, K. Werner, S. A. Sørensen, K. Zamelczyk, E. Kandiano, G. Budeus, K. Husum, T. M. Marchitto, M. Hald, Enhanced Modern Heat Transfer to the Arctic by Warm Atlantic Water. *Science* **331**, 450–453 (2011).
54. F. Lapointe, R. S. Bradley, P. Francus, N. L. Balascio, M. B. Abbott, J. S. Stoner, G. St-Onge, A. de Coninck, T. Labarre, Annually resolved Atlantic sea surface temperature variability over the past 2,900 y. *Proc. Natl. Acad. Sci. U. S. A.* **117**, 27171–27178 (2020).
55. C. Kinnard, C. M. Zdanowicz, D. A. Fisher, E. Isaksson, A. De Vernal, L. G. Thompson, Reconstructed changes in Arctic sea ice over the past 1,450 years. *Nature*. **479**, 509–512 (2011).

56. E. Crespin, H. Goosse, T. Fichefet, M. E. Mann, The 15th century Arctic warming in coupled model simulations with data assimilation. *Clim. Past*. **5**, 389–401 (2009).
57. I. M. Ringgaard, S. Yang, E. Kaas, J. H. Christensen, Barents-Kara sea ice and European winters in EC-Earth. *Clim. Dyn.* **54**, 3323–3338 (2020).
58. K. Sato, J. Inoue, M. Watanabe, Influence of the Gulf Stream on the Barents Sea ice retreat and Eurasian coldness during early winter. *Environ. Res. Lett.* **9** (2014).
59. M. Honda, J. Inoue, S. Yamane, Influence of low Arctic sea-ice minima on anomalously cold Eurasian winters. *Geophys. Res. Lett.* **36**, 1–6 (2009).
60. T. Gong, D. Luo, Ural blocking as an amplifier of the Arctic sea ice decline in winter. *J. Clim.* **30**, 2639–2654 (2017).
61. J. Liu, J. a Curry, H. Wang, M. Song, R. M. Horton, Impact of declining Arctic sea ice on winter snowfall. *Proc. Natl. Acad. Sci.* **109**, 4074–4079 (2012).
62. P. Moffa-Sánchez, A. Born, I. R. Hall, D. J. R. Thornalley, S. Barker, Solar forcing of North Atlantic surface temperature and salinity over the past millennium. *Nat. Geosci.* **7**, 275–278 (2014).
63. M. Schwander, M. Rohrer, S. Brönnimann, A. Malik, Influence of solar variability on the occurrence of Central European weather types from 1763 to 2009. *Clim. Past Discuss.*, 1–25 (2017).
64. C. Martin-Puertas, K. Matthes, A. Brauer, R. Muscheler, F. Hansen, C. Petrick, A. Aldahan, G. Possnert, B. van Geel, Regional atmospheric circulation shifts induced by a grand solar minimum. *Nat. Geosci.* **5**, 397–401 (2012).
65. S. Ineson, A. a. Scaife, J. R. Knight, J. C. Manners, N. J. Dunstone, L. J. Gray, J. D. Haigh, Solar forcing of winter climate variability in the Northern Hemisphere. *Nat. Geosci.* **4**, 753–757 (2011).
66. T. Woollings, M. Lockwood, G. Masato, C. Bell, L. Gray, Enhanced signature of solar variability in Eurasian winter climate. *Geophys. Res. Lett.* **37** (2010)
67. J. A. Eddy, The maunder minimum. *Science* **192**, 1189–1202 (1976).
68. N. V. Zolotova, D. I. Ponyavin, Is the new Grand minimum in progress? *J. Geophys. Res. Sp. Phys.* **119**, 3281–3285 (2014).
69. M. V. Guarino, L. C. Sime, D. Schröeder, I. Malmierca-Vallet, E. Rosenblum, M. Ringer, J. Ridley, D. Feltham, C. Bitz, E. J. Steig, E. Wolff, J. Stroeve, A. Sellar, Sea-ice-free Arctic during the Last Interglacial supports fast future loss. *Nat. Clim. Chang.* **10**, 928–932 (2020).

Acknowledgments: We are thankful for the financial support provided by grants from the Science Vanguard Research Program of the Ministry of Science and Technology (MOST) (110-2123-M-002-009), the National Taiwan University (110L8907 to C.-C.S.), and the Higher Education Sprout Project of the Ministry of Education (110L901001 and 110L8907). We also thank the Japan-Taiwan Exchange Association.

Author contributions: C.-C.S. directed this research. C.-C.S. and H.-M.H. conceived the project. C.-C.S., H.-M.H., E.S., M.Z., V.M. and P.V. conducted field surveys and collected the stalagmite. H.-M.H, W.-Y.C., H.-C.T. and W.-H.S. conducted subsample preparation. H.-M.H, W.-Y.C. and H.-C.T. performed U-Th dating. H.-M.H, T.V., P.C., R.K., J.C.H.C, Y.-T.C. and C.-C.S. prepared the draft and interpretations, and all authors contributed to manuscript completion.

Competing interests: Authors declare no competing interests.

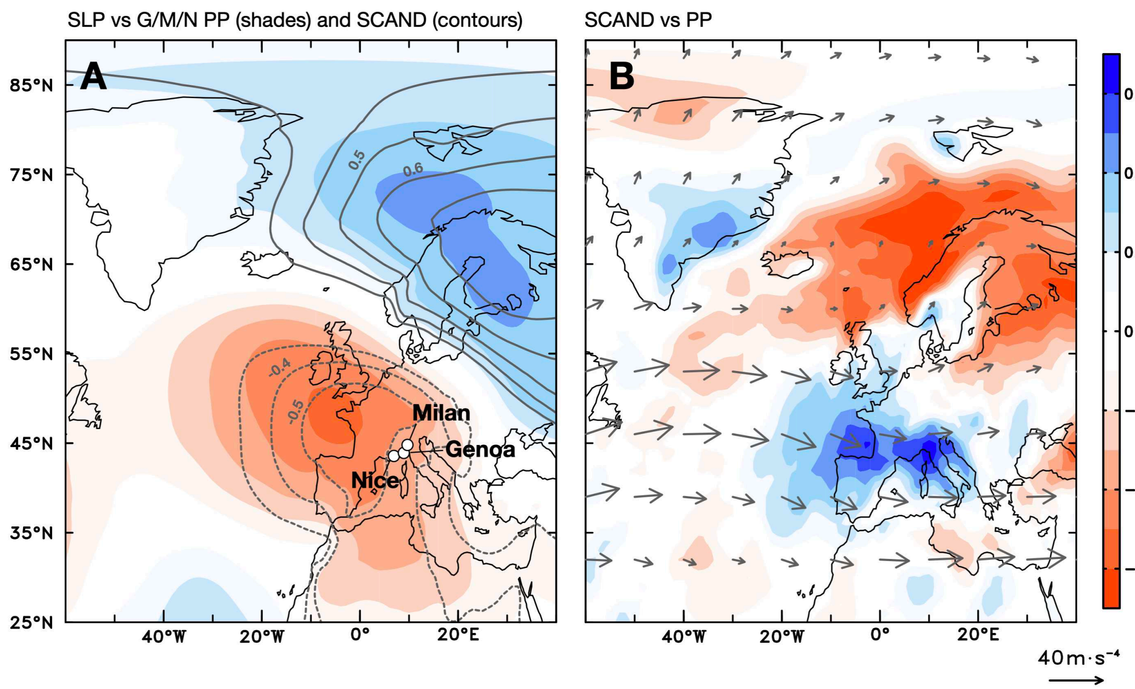

Fig. 1. Climate and Atlantic sea-level pressure (SLP) variability. (A) Correlation between SLP and (i) average precipitation at Genoa, Milan and Nice stations (G/M/N PP) (shades); (ii) Climate Prediction Center (CPC) Scandinavia index (SCAND) (contours) during September-February in 1950-2008 C.E. **(B)** Vectors: climatological winds at 200-mb level plus regression of 200-mb winds on SCAND index multiplied by two standard deviation of SCAND index during September-February in 1950-2008 C.E., indicating a positive SCAND condition. Shades: correlation between SCAND and ground precipitation during September-February in 1950-2008 C.E. The shades and contours indicate the correlation coefficient(s) above 90% confident level. Climate data are from 20 century reanalysis v3.

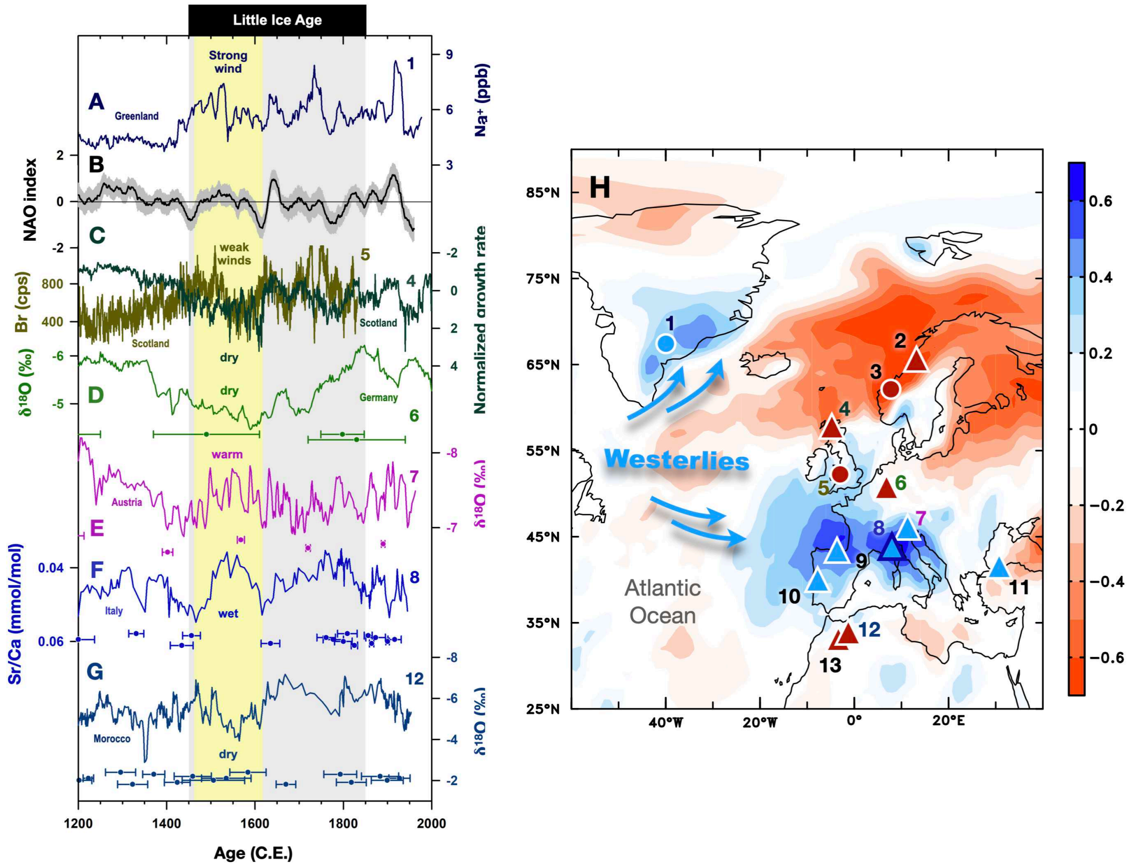

Fig. 2. Climate records from Europe and northern Africa for the last 800 years. (A) Na^+ concentration in ice core GISP2 as an indicator of wind strength. **(B)** Reconstructed NAO index (9). **(C)** Green: Stalagmite growth rate from Roaring cave (Scotland) as a proxy of precipitation amount. Low growth rate indicates positive NAO phase (35). Mustard: Bromine concentration from aeolian sediments as a proxy of wind strength. High values indicate strong winds (28). **(D)** Bunker $\delta^{18}O$ record from Germany (36, 37). Low values reflect a warm and wet climate. **(E)** Spannagel $\delta^{18}O$ record from Austria (40). Low values denote a warm climate. **(F)** Bàsura Sr/Ca record from northern Italy. **(G)** Ifoulki $\delta^{18}O$ record from Morocco (43). Grey vertical band marks the Little Ice Age. The yellow vertical bar highlights the period 1470-1610 C.E. Colored-coded dots and bars are U-Th ages with 2-sigma uncertainties. **(H)** Map showing the climate configuration and location of the cited records. The red-blue shades show the correlation coefficient(s) between SCAND and ground precipitation during September-February in 1950-2008 C.E. Climate data are from 20 century reanalysis v3. Triangles and circles mark westerly-affected sites with a wet/warm (blue) or dry/cold (red) climate. The Bàsura cave is highlighted by a dark blue edge. 1: GISP2 (34). 2: Korallgrottan cave (38). 3: Neflon (39). 4: Roaring cave (35). 5; Outer Hebrides (28). 6: Bunker cave (36, 37). 7: Spannagel cave (40). 8. Bàsura cave. 9: Kaite cave (41). 10: Buraca Gloriosa cave (29). 11: Sofular cave (42). 12: Ifoulki cave (31). 13: Chaara cave (44).

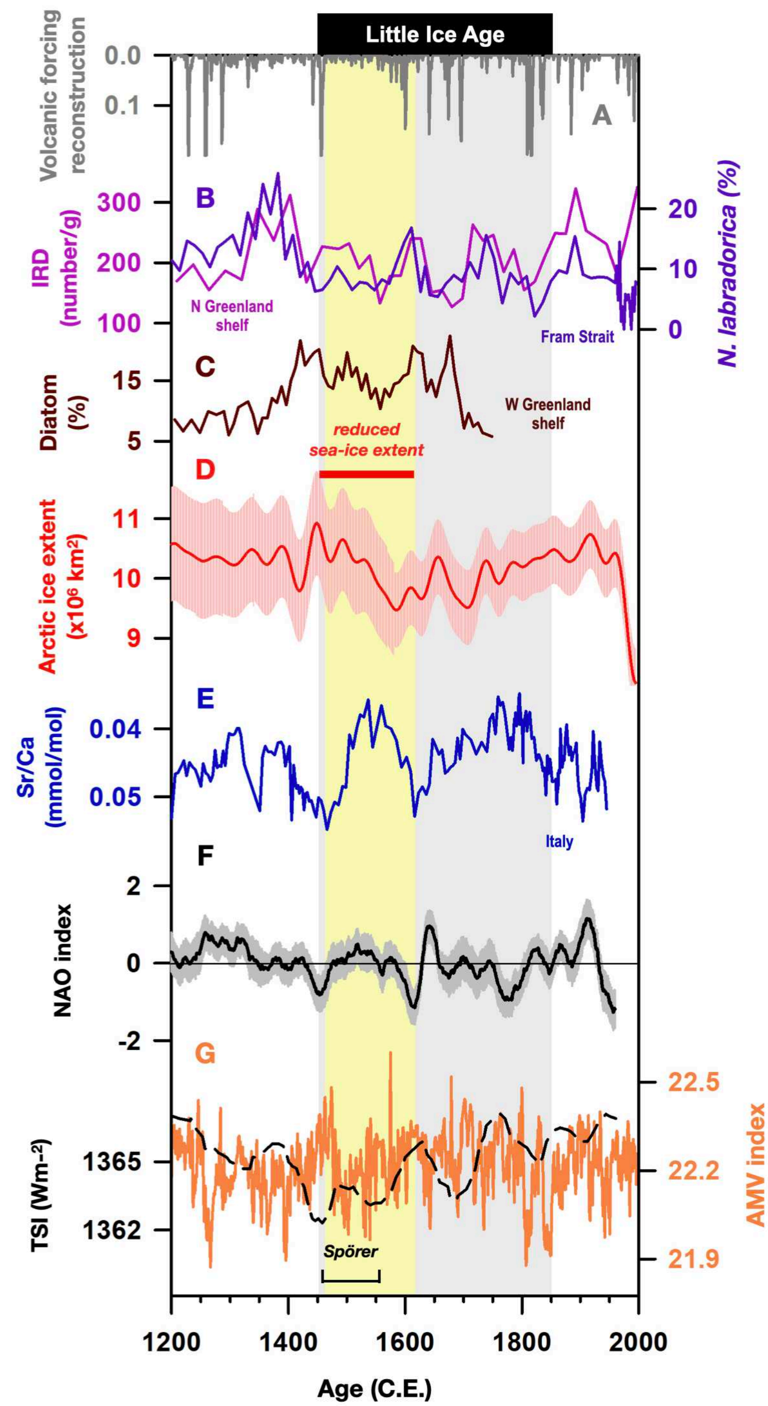

Fig. 3. Comparison of volcanic forcing, solar activity, sea-ice variability and Bàsura records. (A) Simulated volcanic forcing (49). **(B)** Violet: concentration of benthic foraminifera from the North Greenland shelf (PS2641-4; Fig. S1) as an indicator of sea-ice cover (47). Pink:

ice-rafted debris (IRD) (MSM5/5; Fig S1) from the Fram Strait (46). High values of these two records denote large sea-ice cover. **(C)** Five-point averaged diatom concentration (*Thalassiosira nordenskioeldii*) from the west Greenland shelf (GA306-4; Fig S1) (48). High value denotes large sea-ice cover. **(D)** Red: 40-year smoothed reconstructed late summer Arctic sea-ice extent (55). **(E)** Bàsura Sr/Ca record. **(F)** Reconstructed NAO index (9). **(G)** Orange: Atlantic Multidecadal Variability index (54). Black: total solar irradiance (50). The intervals of the Spörer Minimum (1460-1550 C.E.; 67) and decreased sea-ice event (1450-1620 C.E.; 55) are marked. The grey vertical bar denotes the Little Ice Age. The yellow vertical bar highlights the period 1470-1610 C.E.

Supplementary Files

This is a list of supplementary files associated with this preprint. Click to download.

- 2022HunewsuppLIAv7.pdf
- DataS1.TraceelementdataofBA184.xlsx